Journal of Alloys and Compounds 504 (2010) 1–6

Contents lists available at ScienceDirect

Journal of Alloys and Compounds

journal homepage: www.elsevier.com/locate/jallcom

Crystal structure and physical properties of Yb-based intermetallics Yb(Cu, Ag)$_2$(Si, Ge)$_2$, Yb(Cu$_{1-x}$Zn$_x$)$_2$Si$_2$ (x = 0.65, 0.77) and Yb(Ag$_{0.18}$Si$_{0.82}$)$_2$

A. Grytsiv[a,*], D. Kaczorowski[b], V.-H. Tran[b], A. Leithe-Jasper[a], P. Rogl[a]

[a] Institute of Physical Chemistry, University of Vienna, Währingerstrasse 42, A-1090 Wien, Austria
[b] Institute for Low Temperature and Structure Research, Polish Academy of Sciences, P.O. Box 1410, 50-950 Wrocław, Poland

ARTICLE INFO

Article history:
Received 7 March 2010
Received in revised form 6 May 2010
Accepted 7 May 2010
Available online 20 May 2010

Keywords:
Ytterbium intermetallics
Magnetism
Electrical conductivity
Intermediate valent systems

ABSTRACT

X-ray powder data for YbCu$_2$Ge$_2$, YbAg$_2$Si$_2$ and YbAg$_2$Ge$_2$ confirmed the atom order of the ThCr$_2$Si$_2$ type (ordered BaAl$_4$ type) as reported earlier. YbCu$_2$Ge$_2$ is an intermediate valence system with the Yb ions valence close to +2 at low temperatures, whereas the other two compounds are weakly temperature-dependent paramagnets. All these ternaries show metallic character of their electrical conductivity. The structure of Yb(Cu$_{1-x}$Zn$_x$)$_2$Si$_2$ (x = 0.65, 0.77) was found to correspond to the BaAl$_4$ type, assuming a random distribution of Cu and Zn atoms over the positions 4d (0, 1/2, 1/4). The Si atoms were found in the sites 4e (0, 0, z). These two pseudoternary compounds are diamagnetic. A novel phase with the composition Yb(Ag$_{0.18}$Si$_{0.82}$)$_2$ crystallizes in the ThSi$_2$-type on the verge to a symmetry reduction towards orthorhombic GdSi$_2$-type. This phase is a Pauli paramagnet and exhibits metallic behavior of the resistivity.

1. Introduction

Rare earth metal disilicides and digermanides have gained some interest as electric contact materials in Si/Ge-waver based electronic devices [1]. Sharply structured photoluminescence bands from rare earth intra-4f-shell transitions have furthermore spurred interest in optical fibre telecommunication [2]. However, there is still a serious lack of reliable phase equilibria data for the corresponding Si(Ge)-rare earth systems with contact materials, as well as of the crystal structure and the physical properties of the intermediate phases [3]. Our general interest in the physical (magneto-electrical) properties of ternary ytterbium-containing compounds [4–9] and in particular of corresponding silicides/germanides prompted us to study the concentration sections YbSi$_2$ – T and YbGe$_2$ – T, where T is one of the metals Cu, Zn, Ag.

From the ternary compounds YbT$_2$Si$_2$ and YbT$_2$Ge$_2$ with T = Cu, Ag only YbCu$_2$Si$_2$ has intensively been investigated in the past. The compound was reported to be a moderately enhanced heavy fermion system with an electronic specific heat coefficient γ of 135 mJ/(mol K^2) [10], an ytterbium ion valence at 4.2 K of about 2.8 [11,12] and a characteristic Kondo temperature T_K = 200 K [13]. The magnetic susceptibility of YbCu$_2$Si$_2$ follows above 75 K a Curie–Weiss law with a large negative paramagnetic Curie temperature Θ = −90 K and an effective magnetic moment μ_{eff} = 4.19μ_B that is considerably reduced in respect to the free Yb^{3+} ion value [10]. At ambient pressure no long-range magnetic ordering occurs in this compound down to 0.4 K [10]. Most interestingly, application of pressure results in a valence change of Yb ions from the intermediate value to a 3+ state [14] and the system approaches a magnetic instability at the critical pressure of about 8 GPa [15,16].

Recent studies of Yb(Cu$_{0.125}$Si$_{0.875}$)$_{2-x}$ revealed two structural modifications with different physical behavior [17]: whereas the ThSi$_2$-type modification is a new intermediate valent material, the AlB$_2$-type compound shows an enhanced coefficient of the electronic specific heat and physical properties reminiscent of non-Fermi liquid compounds.

These important findings motivated us to undertake investigations of the physical properties of related compounds: YbCu$_2$Ge$_2$, YbAg$_2$Si$_2$ and YbAg$_2$Ge$_2$, which, to the best of our knowledge, have not hitherto been reported in the literature. In the course of our attempts to prepare the YbT$_2$Si$_2$ phases we discovered a novel compound Yb(Ag$_{0.18}$Si$_{0.82}$)$_2$ as well as a pseudoternary system Yb(Cu$_{1-x}$Zn$_x$)$_2$Si$_2$. Moreover, using the Lebeau method [18] we succeeded to grow single crystals of such alloys with x = 0.65 and 0.77. This paper summarizes the results of magnetic and electrical measurements performed on all these materials in a wide range of temperature.

2. Experimental details

Polycrystalline samples of YbCu$_2$Ge$_2$, YbAg$_2$Si$_2$ and YbAg$_2$Ge$_2$, each with a total weight of about 1–2 g, were prepared by repeated arc-melting appropriate amounts

* Corresponding author.
E-mail address: andriy.grytsiv@univie.ac.at (A. Grytsiv).

0925-8388/$ – see front matter © 2010 Elsevier B.V. All rights reserved.
doi:10.1016/j.jallcom.2010.05.051

Table 1
Structural data (Rietveld refinements, *I*4/*mmm*, $ThCr_2Si_2(CeAl_2Ga_2)$-type structure) for $Yb(Cu, Ag, Zn)_2(Si, Ge)_2$ compounds. Data collection: Huber Image Plate; Radiation: $CuK\alpha_1$; 2θ range: $8 \le 2\theta \le 100$[a].

Parameter/compound	$YbAg_2Si_2$	$Yb(Zn_{0.65}Cu_{0.35})_2Si_2$	$YbCu_2Ge_2$
a (nm), Guinier film	0.41900(5)	0.4071(2)	0.40521(9)
c (nm), Guinier film	1.0622(3)	1.028(1)	1.0273(7)
Reflections measured	47	42	41
Number of variables	21	23	21
$R_F = \Sigma\|F_o - F_c\|/\Sigma F_o$	0.038	0.064	0.050
$R_I = \Sigma\|I_o - I_c\|/\Sigma I_o$	0.05	0.078	0.050
$R_{wP} = [\Sigma w_i\|y_{oi} - y_{ci}\|^2/\Sigma w_i\|y_{oi}\|^2]^{1/2}$	0.075	0.093	0.097
$R_P = \Sigma\|y_{oi} - y_{ci}\|/\Sigma\|y_{oi}\|$	0.055	0.066	0.071
$R_e = [(N - P + C)/(\Sigma w_i y^2_{oi})]^{1/2}$	0.036	0.018	0.021
$\chi^2 = (R_{wP}/R_e)^2$	4.35	27.9	19.2
Atom parameters			
Yb, 2a (0, 0, 0), B_{iso}[b]	1.93(3)	1.48(4)	1.40(2)
M1 4d (0, 1/2, 1/4), B_{iso}	2.21(3)	2.30(6)	Cu, 1.70(2)
M2 4e (0, 0, *z*), *z*	Si, 0.3910(3)	0.65Zn + 0.35Cu[c], 0.3903(4)	Ge, 0.38108(7)
B_{iso}	2.09(8)	3.3(1)	1.71(2)

[a] Crystal structure data are standardized using the program Structure Tidy [22].
[b] B_{eq} (B_{iso}) are given in 10^{-2}(nm^2).
[c] Fixed.

of the elemental constituents (Yb: 99.9 mass%, Auer Remy; Cu, Ag: 99.9 mass%, Alfa Aesar; Si, Ge: 99.99 mass%, Alfa Ventron). The syntheses were carried out on a water-cooled copper hearth under Ti-gettered high purity argon. All weight losses were attributed to evaporation of Yb and compensated accordingly. Parts of the melted buttons were vacuum-sealed in quartz capillaries and annealed at 600–900 °C for up to 140 h prior to quenching in cold water. These annealed specimens were used for X-ray powder diffraction investigations.

Polycrystalline specimens of $Yb(Cu_{1-x}Zn_x)_2Si_2$ were prepared by powder metallurgy technique. Arc-melted master alloys $YbCu_{2-x}Si_2$ were powdered under cyclohexane and mixed with freshly milled Zn powder (5 N, Alcan Electronics). The compacted powder blends were sealed in evacuated silica ampoules, heat treated at 350–400 °C for 2 days, and finally sintered at 700 °C for 3 days.

Single crystals of $Yb(Cu_{1-x}Zn_x)_2Si_2$ were obtained via the Lebeau method [18], essentially based on the temperature-dependent solubility of the constituting elements in the Zn flux. The substrates were placed in an Al_2O_3 crucible, which was then vacuum-sealed within a thick-walled quartz tube. The tube was heated up to 1050–1100 °C with a rate of 75 °C/h with an intermediate hold at 450 °C for 1 h, i.e. slightly above the melting point of the flux. After a soaking period at the maximum temperature for up to 12 h, cooling to 600 °C proceeded at a speed of 10 °C/h, after which the sample was kept at 600 °C for 12 h prior to final quenching. After removing the Zn flux by 3 N HCl water solution well-developed single crystals could easily be isolated.

Crystal structure identification and rough determination of the unit cell dimensions were performed using a 57.3 mm radius Gandolfi-camera. Weissenberg photographs accomplished crystal quality control and inspection of crystal symmetry. The precise lattice parameters and standard deviations were obtained by a least squares refinement of the room temperature X-ray powder diffraction data, collected on a Guinier-Huber camera with $CuK\alpha_1$ radiation. In these measurements either bulk materials or powdered single crystals (optically selected under a microscope) were used, and 99.9999 mass% pure Ge (a_{Ge} = 0.5657906 nm) or Si (a_{Si} = 0.5431065 nm) served as internal standards. Quantitative refinements of the atom positions were done using the FULLPROF program [19], based on the X-ray intensity data obtained with a Guinier-Huber Image Plate recording system ($CuK\alpha_1$).

Magnetic measurements were performed in the temperature range 1.72–600 K and in magnetic fields up to 5 T using a Quantum Design MPMS-5 SQUID magnetometer. In these studies polycrystalline samples of $YbCu_2Ge_2$, $YbAg_2Si_2$, $YbAg_2Ge_2$ and $Yb(Ag_{0.18}Si_{0.82})_2$ were used. In the case of $Yb(Cu_{1-x}Zn_x)_2Si_2$ collections of single crystals freely placed in a sample holder were used as specimens. The electrical resistivity of $YbCu_2Ge_2$, $YbAg_2Si_2$, $YbAg_2Ge_2$ and $Yb(Ag_{0.18}Si_{0.82})_2$ was measured in the temperature range 4.2–300 K employing a conventional dc four-point technique. In these measurements the electrical leads were attached to bar-shaped polycrystalline specimens by silver-epoxy paste.

3. Results and discussion

3.1. Crystal structures

For $YbAg_2Si_2$, $YbCu_2Ge_2$ and $YbAg_2Ge_2$ systematic extinctions characteristic for body centring and the appropriate unit cell dimensions suggested isotypism with the tetragonal $BaAl_4$ type of structure. Assuming an atomic arrangement corresponding to the $ThCr_2Si_2$ type (ordered variant of $BaAl_4$) satisfactory description of the Guinier X-ray diffraction patterns was obtained for all the materials, in agreement with previous reports on $YbAg_2Si_2$ [20] and $YbCu_2Ge_2$ [21]. $YbAg_2Ge_2$, however, is a new compound of the $ThCr_2Si_2$ type. Results of the Rietveld refinements are summarized in Table 1.

Similarly, the crystal structure of the $Yb(Cu_{1-x}Zn_x)_2Si_2$ pseudoternaries was found to correspond fully with the atomic arrangement of the $BaAl_4$ type in which Yb atoms occupy the 2a positions at the corners and at the centre of the unit cell, Si atoms are at the sites 4e (0, 0, *z*), while Cu and Zn atoms are randomly distributed over the positions 4d (0, 1/2, 1/4). Fig. 1 presents the lattice parameters of the sintered $Yb(Cu_{1-x}Zn_x)_2Si_2$ alloys as a function of Zn content *x*. Despite both lattice parameters change with *x* in a nonlinear fashion, the volume of the unit cell closely obeys Vegard's law. The compositional dependence of the unit cell volume was used to establish compositions of the single crystals grown from Zn flux to be $Yb(Cu_{0.35}Zn_{0.65})_2Si_2$ and $Yb(Cu_{0.23}Zn_{0.77})_2Si_2$ (note full circles in Fig. 1).

Whereas the as-cast alloy "$YbAg_2Si_2$" is multiphase – revealing $YbAg_2Si_2$, a $ThSi_2$-type phase and a (Ag + Si) eutectic – the same alloy turns single-phase $YbAg_2Si_2$ after anneal at 850 °C. As the alloy stays multiphase after anneal at 900 °C, the $YbAg_2Si_2$ phase forms below a temperature between 850 and 900 °C. It is interesting to note, that the $YbAg_2Si_2$ phase was identified by Rossi et al. [20] from a three-phase sample for which the applied annealing procedure (500 °C, 1 week) was obviously insufficient to reach equilibrium. The $ThSi_2$-type phase, observed in the as-cast and multiphase alloy "$YbAg_2Si_2$", was found in single-phase condition at the composition $Yb(Ag_{0.18}Si_{0.82})_2$. The Rietveld refinement with *R*-values as low as 4% shows a random distribution of Ag + Si atoms. Careful analyses of the peak profile structure and the peak widths reveal a slight orthorhombic distortion as encountered in the closely related $GdSi_2$-type. Refinement in orthorhombic symmetry, however, does not lead to any significant lowering of the residual value. The results of the refinements are summarized in Table 2, where for comparison the refinements in both crystal symmetries are listed.

3.2. Magnetic properties

The magnetic behavior of the $Yb(Cu_{1-x}Zn_x)_2Si_2$ alloys with $x = 0.65$, 0.77 is shown in Fig. 2. Both materials are diamagnetic at room temperature with the susceptibility of the order of 10^{-4} emu/mol, indicating that the ytterbium ions are here in a diva-

Table 2
Structural data for $Yb(Si_{0.82}Ag_{0.18})_2$. Data collection: Huber Image Plate; Radiation: CuKα_1; 2θ range: $8 \le 2\theta \le 100$[a].

Parameter/nom. composition	$Yb(Si_{0.813}Ag_{0.187})_2$	$Yb(Si_{0.813}Ag_{0.187})_2$
Composition from refinement	$Yb(Si_{0.830}Ag_{0.170})_2$	$Yb(Si_{0.824}Ag_{0.176})_2$
Space group	$I4_1/amd$	$Imma$
Prototype	$ThSi_2$	$GdSi_2$
a (nm), Image plate	0.408709(5)	0.408307(4)
b (nm), Image plate	1.43069(2)	0.409115(5)
c (nm), Image plate	1.43069(2)	1.43072(1)
Reflections measured	46	93
Number of variables	19	24
$R_F = \Sigma\|F_o - F_c\|/\Sigma F_o$	0.032	0.035
$R_I = \Sigma\|I_o - I_c\|/\Sigma I_o$	0.045	0.042
$R_{wP} = [\Sigma w_i\|y_{oi} - y_{ci}\|^2/\Sigma w_i\|y_{oi}\|^2]^{1/2}$	0.086	0.069
$R_P = \Sigma\|y_{oi} - y_{ci}\|/\Sigma\|y_{oi}\|$	0.058	0.049
$R_e = [(N - P + C)/(\Sigma w_i y^2{}_{oi})]^{1/2}$	0.017	0.017
$\chi^2 = (R_{wP}/R_e)^2$	24.5	15.8
Atom parameters		
Yb	4a (0, 3/4, 1/8)	4e (0, 1/4, 0.6245(1))
B_{eq} (B_{iso}) 10^2(nm^2)	0.46(2)	0.46(1)
Si + Ag	8e (0, 1/4, 0.29128(7))	4e (0, 1/4, 0.2088(4))
occ., B_{eq} (B_{iso}) 10^2(nm^2)	0.83Si + 0.17Ag, 0.53(3)	0.90Si + 0.10Ag, 0.47(2)
Si + Ag	–	4e (0, 1/4, 0.0414(3))
occ., B_{eq} (B_{iso}) 10^2(nm^2)	–	0.75Si + 0.25Ag, 0.50(1)

[a]Crystal structure data are standardized using the program Structure Tidy [22].

lent state. With decreasing temperature $\chi(T)$ exhibits first a slight increase and then a rapid upturn is observed at the lowest temperatures. This effect in the samples studied is probably caused by the presence of small amount of paramagnetic impurities, most likely some ytterbium oxide on the surface of single crystals measured. In order to account for the impurity content the experimental data

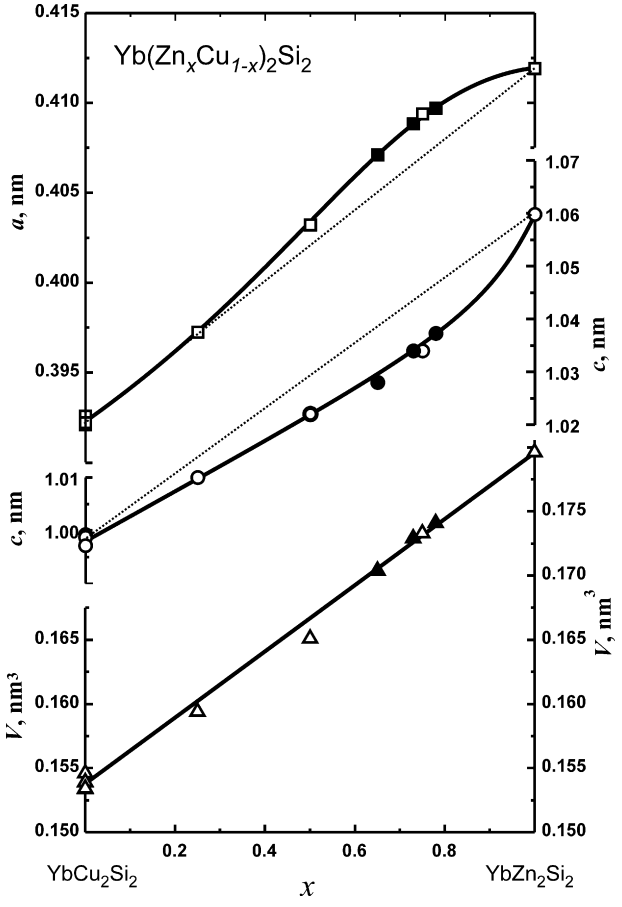

Fig. 1. Compositional dependence of the lattice parameters and the unit cell volume in the $Yb(Cu_{1-x}Zn_x)_2Si_2$ system. The full symbols denote the values derived for the single crystals grown from Zn flux.

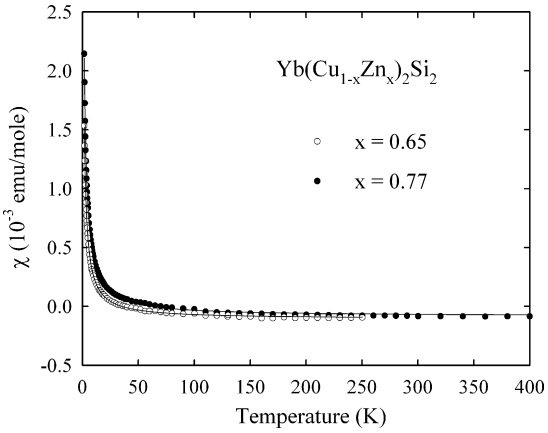

Fig. 2. Temperature dependencies of the molar magnetic susceptibility of $Yb(Cu_{0.35}Zn_{0.65})_2Si_2$ (open circles) and $Yb(Cu_{0.23}Zn_{0.77})_2Si_2$ (full circles), measured in a field of 0.5 T. The thick solid lines are fits of the experimental data to Eq. (1) with the parameters given in the text.

were thus analyzed in terms of the formula

$$\chi(T) = \chi_0 + \chi_{imp}(T) \quad (1)$$

where χ_0 stands for the intrinsic susceptibility of $Yb(Cu_{1-x}Zn_x)_2Si_2$ being the sum of core-electron diamagnetic and conduction-electron paramagnetic contributions, whilst the impurity contribution $\chi_{imp}(T)$ is given by a Curie–Weiss law

$$\chi_{imp}(T) = \frac{C_{imp}}{T - \theta_{imp}}. \quad (2)$$

Fitting the above equations to the experimental data yields the parameters: $\chi_0 = -1.07 \times 10^{-4}$ emu/mol, $C_{imp} = 0.004$ emu K/mol and $\theta_{imp} = -0.7$ K for $Yb(Cu_{0.35}Zn_{0.65})_2Si_2$ and $\chi_0 = -0.84 \times 10^{-4}$ emu/mol, $C_{imp} = 0.005$ emu K/mol and $\theta_{imp} = -0.7$ K for $Yb(Cu_{0.23}Zn_{0.77})_2Si_2$. Assuming that the impurity contribution comes exclusively from uncompensated Yb^{3+} ions one may estimate the impurity concentration: $n = C_{imp}/C_{Yb^{3+}}$ ($C_{Yb^{3+}} = \mu_{eff}^2/8$; $\mu_{eff} = 4.54\mu_B$) to be of about 0.2 at% per mole for both alloys.

Fig. 3 summarizes the magnetic properties of the compounds $YbCu_2Ge_2$, $YbAg_2Si_2$ and $YbAg_2Ge_2$. Common to all three ternaries is the small positive value of the molar susceptibility taken at room

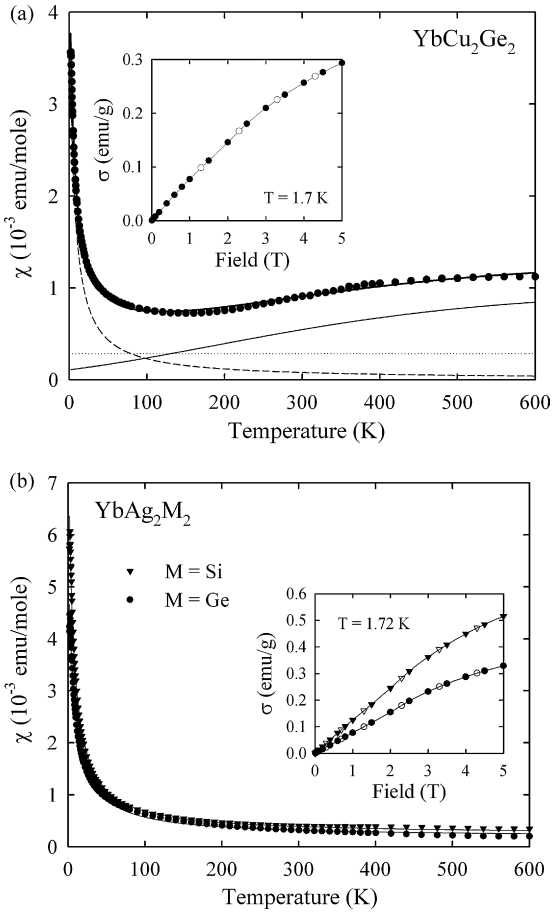

Fig. 3. Temperature dependence of the molar magnetic susceptibility of (a) $YbCu_2Ge_2$, (b) $YbAg_2Si_2$ and $YbAg_2Ge_2$, measured in a field of 0.5 T. In panel (a) the thick solid line is a fit of the experimental data to Eqs. (2)–(5) with the parameters given in the text. The thin solid, dashed and dotted curves represent the functions $\chi_{IV}(T)$, $\chi_{imp}(T)$ and χ_0, respectively. The solid lines in panel (b) are fits of the experimental data to Eq. (1) with the parameters given in the text. Insets: magnetic field variations of the magnetization taken at 1.72 K with increasing (full circles) and decreasing (open circles) magnetic field.

temperature, rather weak temperature dependence $\chi(T)$ (except for temperatures below ca. 100 K), and a paramagnetic-like field variation of the low-temperature magnetization that also shows small magnitude even in the strongest fields applied. Additionally, in the case of $YbCu_2Ge_2$ one observes a non-monotonic behavior in $\chi(T)$ which shows a rise of the susceptibility at elevated temperatures, characteristic of intermediate valence systems. Assuming that the compound contains Yb ions with noninteger valence its susceptibility may be described in the framework of the interconfiguration fluctuation model (ICF) [23] by the formula

$$\chi_{IV}(T) = \frac{N\mu_{eff}^2[1-\nu(T)]}{3k_B(T+T_{sf})} \quad (3)$$

where $\nu(T)$ is a temperature-dependent mean occupation of the ground state

$$\nu(T) = \frac{1}{1+8\,\exp[-E_{ex}/k_B(T+T_{sf})]} \quad (4)$$

the effective magnetic moment $\mu_{eff} = 4.54\mu_B$, T_{sf} stands for the spin fluctuation temperature that characterises the system and E_{ex} is the energy separation of the nonmagnetic $4f^{14}$ ground state configuration from the magnetic $4f^{13}$ excited state. Alike in the above-discussed nonmagnetic alloys the susceptibility upturn at low temperatures presumably arises because of paramagnetic

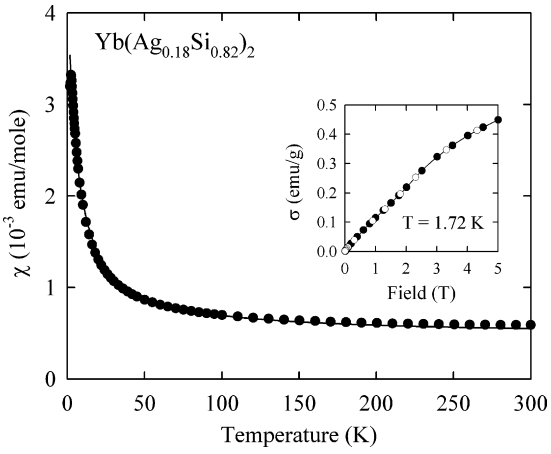

Fig. 4. Temperature dependence of the molar magnetic susceptibility of $Yb(Ag_{0.18}Si_{0.82})_2$, measured in a field of 0.5 T. The solid line is a fit of the experimental data to Eq. (1) with the parameters given in the text.

impurities and hence the measured susceptibility is expressed by the sum

$$\chi(T) = \chi_{IV}(T) + \chi_{imp}(T) + \chi_0 \quad (5)$$

with the terms χ_0 and $\chi_{imp}(T)$ as defined above. The least squares fit of the experimental data of $YbCu_2Ge_2$ to the Eqs. (2)–(5) (see Fig. 3(a)) gives the parameters: $T_{sf} = 489$ K, $E_{ex} = 2908$ K, $C_{imp} = 0.024$ emu K/mol, $\theta_{imp} = -5.4$ K and $\chi_0 \approx 2.8 \times 10^{-4}$ emu/mol. The impurity concentration n estimated from the value of C_{imp} is about 0.9 at% Yb^{3+} ions per mole. The energy E_{ex} is quite large thus indicating that the magnetic $4f^{13}$ configuration is quite distant in energy from the nonmagnetic $4f^{14}$ ground state. The ICF model yields at 2 K the effective valence of the ytterbium atom in $YbCu_2Ge_2$ of only 2.02. With increasing temperature the excited state becomes thermally populated and the valence increases, reaching at 600 K a value of 2.37.

In the case of $YbAg_2Si_2$ and $YbAg_2Ge_2$ no hint at unstable valence of Yb ions is observed (cf. Fig. 3(b)). Hence, the experimental $\chi(T)$ curves were analyzed in terms of Eqs. (1) and (2). The so-derived parameters are as follows: $\chi_0 = 2.36 \times 10^{-4}$ emu/mol, $C_{imp} = 0.048$ emu K/mol and $\theta_{imp} = -5.9$ K for the silicide and $\chi_0 = 1.87 \times 10^{-4}$ emu/mol, $C_{imp} = 0.041$ emu K/mol and $\theta_{imp} = -7.4$ K for the germanide. From the values of C_{imp} one finds the concentration of impurities to be about 1.8 and 1.6 at% Yb^{3+} ions per mole in $YbAg_2Si_2$ and $YbAg_2Ge_2$, respectively, i.e. considerably larger than in the other samples studied, yet still below the detection limit of X-ray diffraction technique.

As displayed in Fig. 4, nonmagnetic behavior was revealed also for the compound $Yb(Ag_{0.18}Si_{0.82})_2$. In this case the fitting of Eqs. (1) and (2) to the experimental data yields the parameters: $\chi_0 = 4.75 \times 10^{-4}$ emu/mol, $C_{imp} = 0.023$ emu K/mol and $\theta_{imp} = -5.9$ K. From these results the amount of Yb^{3+} ions considered as the impurity contribution in the nominally Pauli paramagnetic sample measured is 0.9 at% per mole.

3.3. Electrical properties

The temperature variations of the electrical resistivity of $YbCu_2Ge_2$, $YbAg_2Si_2$ and $YbAg_2Ge_2$ are shown in Fig. 5. All three compounds exhibit metallic character of the electrical conduction with the resistivity of few tens μΩ cm at room temperature. The $\rho(T)$ curves are featureless down to 4.2 K, in line with nonmagnetic character of the materials studied. At low temperatures (below ca. 60 K) the resistivity varies as AT^2 (see the insets in Fig. 5) with the coefficient A being equal to 10.2×10^{-4}, 2.8×10^{-4}

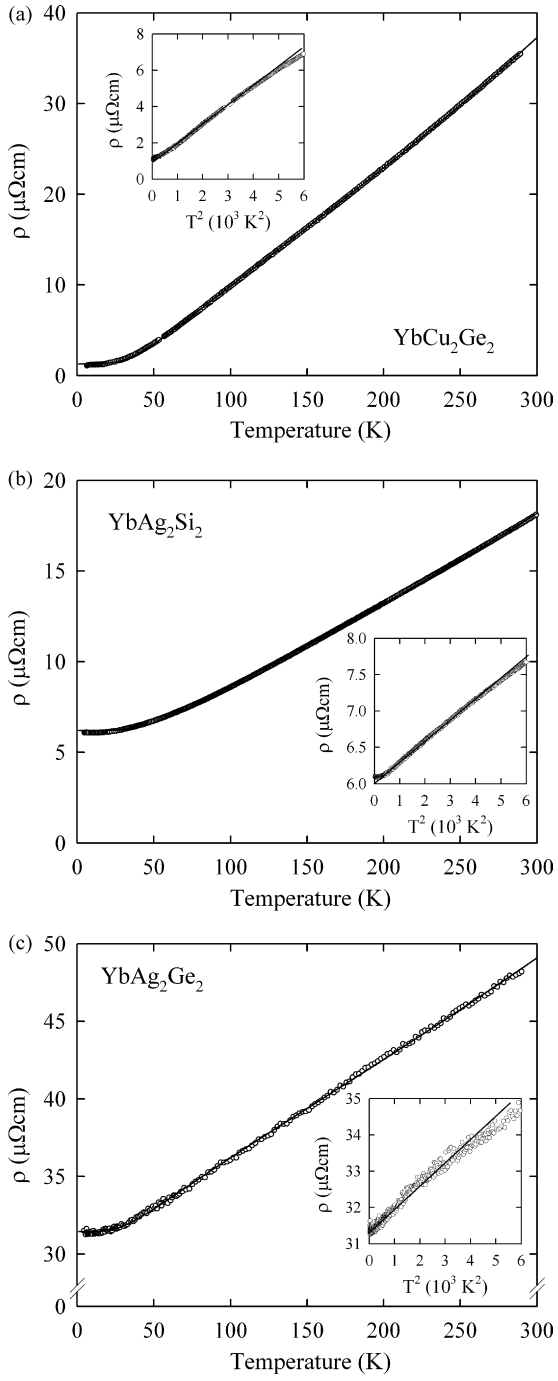

Fig. 5. Temperature dependence of the electrical resistivity of (a) $YbCu_2Ge_2$, (b) $YbAg_2Si_2$, and (c) $YbAg_2Ge_2$. In each panel the solid line is a fit of the experimental data to Eq. (6) with the parameters given in the text. Insets: low-temperature resistivity plotted as a function of squared temperature. The solid lines mark T^2 variations.

and 6.7×10^{-4} μΩ cm/K^2 for $YbCu_2Ge_2$, $YbAg_2Si_2$ and $YbAg_2Ge_2$, respectively. According to the Kadowaki–Woods scaling [24] these values correspond to the electronic coefficient of the specific heat γ of about 10, 8 and 5 mJ/(mol K^2), respectively. Slightly enhanced γ for $YbCu_2Ge_2$ is consistent with the intermediate valent character of this germanide [25].

In the entire temperature range for the $\rho(T)$ curves may be well approximated by the Bloch–Grüneisen–Mott (BGM) formula [26] that comprises residual, phonon, and interband scattering contributions

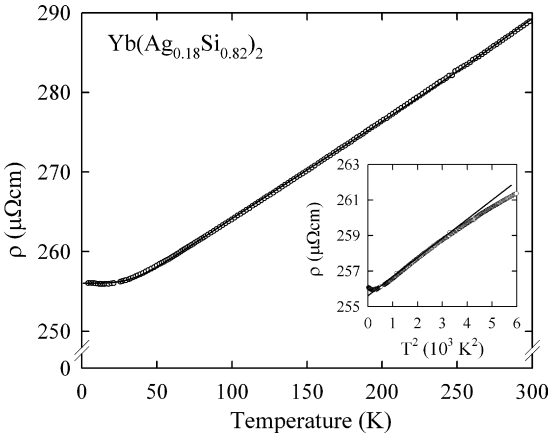

Fig. 6. Temperature dependence of the electrical resistivity of $Yb(Ag_{0.18}Si_{0.82})_2$. The solid line is a fit of the experimental data to Eq. (6) with the parameters given in the text. Inset: low-temperature resistivity plotted as a function of squared temperature. The solid line marks a T^2 variation.

$$\rho = \rho_0 + 4R\theta_D\left(\frac{T}{\theta_D}\right)^5 \int_0^{\theta_D/T} \frac{x^5 dx}{(e^x - 1)(1 - e^{-x})} + KT^3 \qquad (6)$$

with the parameters: $\rho_0 = 1.3$ μΩ cm, $\Theta_D = 218$ K, $R = 0.108$ μΩ cm/K and $K = 1.6 \times 10^{-7}$ μΩ cm/K^3 for $YbCu_2Ge_2$, $\rho_0 = 6.2$ μΩ cm, $\Theta_D = 292$ K, $R = 0.037$ μΩ cm/K and $K = 5.5 \times 10^{-8}$ μΩ cm/K^3 for $YbAg_2Si_2$, and $\rho_0 = 31.4$ μΩ cm, $\Theta_D = 182$ K, $R = 0.056$ μΩ cm/K and $K = 3.9 \times 10^{-8}$ μΩ cm/K^3 for $YbAg_2Ge_2$. The Debye temperature derived for $YbCu_2Ge_2$ is very close to the value reported for $YbCu_2Si_2$ ($\Theta_D = 221$ K [10]). For all three compounds studied Mott's term is very small and does not affect considerably a nearly linear behavior of $\rho(T)$ above about 100 K.

Fig. 6 presents the temperature dependence of the electrical resistivity of $Yb(Ag_{0.18}Si_{0.82})_2$. In comparison to the case of the $Yb(Cu, Ag)_2(Si, Ge)_2$ compounds, the resistivity is an order of magnitude larger in the entire temperature range. This feature clearly reflects an atomic disorder in the unit cell, where two crystallographic positions have mixed occupancies of Ag and Si atoms (see Table 2). The overall behavior of the $\rho(T)$ curve is however very similar to the afore-discussed data. The A coefficient in the T^2 variation of the resistivity (observed in the interval 15–50 K) amounts to 11.0×10^{-4} μΩ cm/K^2 that provides an estimate for the Sommerfeld coefficient of 10 mJ/(mol K^2). The BGM formula can be well fitted to the experimental data yielding the parameters: $\rho_0 = 256$ μΩ cm, $\Theta_D = 222$ K, $R = 0.104$ μΩ cm/K and $K = 1.1 \times 10^{-7}$ μΩ cm/K^3, i.e. close (except for ρ_0) to those found for the other intermetallics studied. Below about 15 K, the $\rho(T)$ curve shows a little upturn (cf. the inset to Fig. 6) that likely arises due to the presence of some Yb^{3+} ions, revealed in the magnetic data, which behave as single Kondo impurities in the nominally nonmagnetic $Yb(Ag_{0.18}Si_{0.82})_2$ compound.

4. Summary

The magnetic measurements revealed that $YbAg_2Si_2$, $YbAg_2Ge_2$ and $Yb(Ag_{0.18}Si_{0.82})_2$ are weak Pauli paramagnets, whereas the two studied $Yb(Cu_{1-x}Zn_x)_2Si_2$ pseudoternary alloys ($x = 0.65$, 0.77) exhibit weak diamagnetism. In all these systems the ytterbium ions are in divalent states. In turn, for $YbCu_2Ge_2$ an intermediate valent character of the magnetic susceptibility was found thus indicating that the valence state of the Yb ions in this compound is unstable. Similar behavior has previously been observed for the corresponding silicide $YbCu_2Si_2$ [10–12]. However, in contrast to the latter

phase that exhibits the Yb valence of 2.9 at room temperature and decreases to 2.8 at $T = 4.2$ K [11], i.e. it is close to 3+ in the wide temperature range, the Yb valence in the germanide is only 2.02 at $T = 1.7$ K and rises to 2.37 at high temperature of 600 K, i.e. it is close to divalent state. This distinct difference in the valence states is clearly reflected in the thermal behavior of the magnetic susceptibility that in the case of $YbCu_2Si_2$ follows the Curie–Weiss law with a large effective magnetic moment of 4.19 μ_B [10], and keeps a non-Curie–Weiss character up to very high temperatures in the case of $YbCu_2Ge_2$. In line with a nearly nonmagnetic character of $YbCu_2Ge_2$, the electronic correlations in this material are rather weak, as indicated by only minor enhancement of the electronic specific heat, estimated from the electrical resistivity data.

Acknowledgement

This research was supported by the Austrian-Polish Scientific-Technical Exchange Program under project PL 06/2009.

References

[1] J. Nogami, Rare Earth Metal/Semiconductor Interfaces and Compounds, Thesis, Stanford, CA, Univ. Microfilms order No. 86-12. 776 (1986) 1-206;
see also J. Nogami, C. Carbone, D.J. Friedman, I. Lindau, Phys. Rev. B 33 (1986) 864.
[2] Y. Yang, H. Chen, Y.Q. Zhou, F.H. Li, J. Mater. Sci. 32 (1997) 6665.
[3] P. Villars, A. Prince, H. Okamato, Handbook of Ternary Alloy Phase Diagrams, vols. 1–10, ASM International, Materials Park, OH, USA, 1995.
[4] A. Grytsiv, A. Leithe-Jasper, H. Flandorfer, P. Rogl, K. Hiebl, C. Godart, T. Velikanova, J. Alloys Compd. 266 (1998) 7.
[5] A. Grytsiv, D. Kaczorowski, A. Leithe-Jasper, V.H. Tran, A. Pikul, P. Rogl, M. Potel, H. Noel, M. Bohn, T. Velikanova, J. Solid State Chem. 163 (2002) 178.
[6] A. Grytsiv, D. Kaczorowski, A. Leithe-Jasper, P. Rogl, M. Potel, H. Noel, A. Pikul, T. Velikanova, J. Solid State Chem. 165 (2002) 178.
[7] D. Kaczorowski, A. Leithe-Jasper, P. Rogl, H. Flandorfer, T. Cichorek, R. Pietri, B. Andraka, Phys. Rev. B 60 (1999) 422.
[8] B. Andraka, R. Petri, D. Kaczorowski, A. Leithe-Jasper, P. Rogl, J. Appl. Phys. 87 (2000) 5149.
[9] E. Bauer, A. Galatanu, H. Michor, G. Hilscher, P. Rogl, P. Boulet, H. Noël, Eur. Phys. J. 14 (2000) 483.
[10] B.C. Sales, R. Wiswanathan, J. Low Temp. Phys. 23 (1976) 449.
[11] G. Neumann, J. Langen, H. Zahel, D. Plumacher, Z. Kletowski, W. Schlabitz, D. Wohlleben, Z. Phys. B 59 (1985) 133.
[12] M.N. Groshev, M.D. Koterlin, E.M. Levin, R.V. Lutsiv, N.M. Miftakhov, Yu.P. Smirnov, A.E. Sovestnov, A.V. Tyunis, V.A. Shaburnov, R.I. Yasnitskii, S.M. Kuzmina, V.I. Petrova, V.A. Tyukavin, Sov. Phys. Solid State 28 (9) (1987) 1519.
[13] K. Tomala, D. Weschenfelder, G. Czjzer, E. Holland-Moritz, J. Magn. Magn. Mater. 89 (1990) 143.
[14] U. Walter, E. Holland-Moritz, U. Steigenberger, Z. Phys. B 89 (1992) 169.
[15] K. Alami-Yadri, D. Jaccard, Solid State Commun. 100 (1996) 385.
[16] K. Alami-Yadri, H. Wilhelm, D. Jaccard, Eur. Phys. J. B 6 (1998) 5.
[17] V.H. Tran, D. Kaczorowski, A. Gritsiv, P. Rogl, Physica B 378–380 (2006) 163.
[18] P. Lebeau, J. Figueras, C.R. Acad. Sci., Paris 136 (1903) 1329.
[19] J. Rodriguez-Carvajal, FULLPROF: A Program for Rietveld Refinement and Pattern Matching Analysis, Physica B 192 (1993) 55.
[20] D. Rossi, M. Marazza, R. Ferro, J. Less Common Met. 66 (1979) P17.
[21] W. Rieger, E. Parthé, Monatsh. Chem. 100 (1969) 444.
[22] E. Parthé, L. Gelato, B. Chabot, M. Penzo, K. Cenzual, R. Gladyshevskii, Typix-Standardized Data and Crystal Chemical Characterization of Inorganic Structure Types, vol. 1, p. 233, Table E52; Gmelin Handbook of Inorganic and Organometallic Chemistry, 8th Editions, Springer-Verlag, 1993.
[23] B.C. Sales, D.K. Wohlleben, Phys. Rev. Lett. 35 (1975) 1240.
[24] K. Kadowaki, S.B. Woods, Solid State Commun. 58 (1986) 507.
[25] J.M. Lawrence, P.S. Riseborough, R.D. Parks, Rep. Prog. Phys. 44 (1981) 1.
[26] N.F. Mott, H. Jones, The Theory of the Properties of Metals and Alloys, Oxford University Press, London, 1958.